Global Jack-Up Rig Behaviour Next to a Footprint

M. J. Jun[1], Y. H. Kim[2], M. S. Hossain[3], M. J. Cassidy[4], Y. Hu[5] and S. G. Park[6]

[1]PhD Student, Centre for Offshore Foundation Systems (COFS), Oceans Graduate School, The University of Western Australia, 35 Stirling Highway, Crawley, WA 6009, Australia, Tel: +61 (0)8 6488 7725, Email: minjung.jun@research.uwa.edu.au

[2]Corresponding Author, Research Fellow (PhD), Centre for Offshore Foundation Systems (COFS), Oceans Graduate School, The University of Western Australia, 35 Stirling Highway, Crawley, WA 6009, Australia, Tel: +61 (0)8 6488 4316, Email: youngho.kim@uwa.edu.au

[3]Associate Professor (BEng, MEng, PhD, MIEAust), Centre for Offshore Foundation Systems (COFS), Oceans Graduate School, The University of Western Australia, 35 Stirling Highway, Crawley, WA 6009, Australia, Tel: +61 (0)8 6488 7358, Email: muhammad.hossain@uwa.edu.au

[4]Professor (FTSE, FIEAust, GAICD, DPhil), Dean and Professor of Civil Engineering, Melbourne School of Engineering, Doug McDonell Building, The University of Melbourne, Victoria 3010, Australia, Tel: +61 3 8344 6619, Email: mark.cassidy@unimelb.edu.au

[5]Professor (PhD, MIEAust), School of Civil, Environmental and Mining Engineering, The University of Western Australia, 35 Stirling Highway, Crawley, WA 6009, Australia, Tel: +61 (0)8 6488 8182, Email: yuxia.hu@uwa.edu.au

[6]Senior Research Engineer (MS), Daewoo Shipbuilding & Marine Engineering Co. Ltd. (DSME), 96, Baegot 2-ro, Siheung-si, Gyeonggi-do, Republic of Korea Tel: +82 (0)31 2129 3598, Email: sgpark8@dsme.co.kr

- Number of Words: 5315 (text only)
- Number of Tables: 04
- Number of Figures: 20

Global Jack-Up Rig Behaviour Next to a Footprint

ABSTRACT

This paper reports the effect of the global behaviour of three-legged jack-up rigs due to the reinstallation of spudcan footings next to seabed footprints. Two reinstallation scenarios are discussed: (i) two legs first installed on flat ground, and then the third leg installed near a footprint (representing what is known as leg-by-leg preloading); and (ii) the three legs installed simultaneously (representing simultaneous preloading). The spudcan-soil interaction was simulated using a coupled Eulerian-Lagrangian (CEL) approach. A simplified global jack-up model was developed by considering an equivalent beam model for the hull and legs. The results of the jack-up installations are compared against the responses of the more common modelling of a spudcan with a fixed head condition. A detailed parametric study assessing the consequences of spudcan-footprint interactions, such as the risk of the jack-up and spudcan sliding towards the footprint centre, overturning of the jack-up rig and of structural failure of the jack-up leg due to excessive stresses, is also discussed. The ability of a recently developed novel spudcan with a flat base and 4 holes, coupled with the global jack-up model, to mitigate the consequences of spudcan-footprint interactions is highlighted.

Keywords: jack-up, spudcan-footprint interaction, spudcan, global behaviour, numerical modelling

1. INTRODUCTION

Most offshore drilling in shallow to moderate water is performed from self-elevating jack-up rigs due to their proven flexibility, mobility and cost-effectiveness [1,2]. Modern jack-ups typically consist of a buoyant triangular platform supported by three independent truss legs, each attached to a large-diameter spudcan. Jack-ups often return to sites where previous operations have left footprints in the seabed. As shown in Fig. 1, if one of the jack-up legs is located near a footprint slope, there is a tendency for the spudcan to slide towards the centre of the footprint, inducing excessive lateral displacements and bending moments or rotations in the rig. These detrimental foundation behaviours can result in an inability to install the jack-up in the required position, the occurrence of leg splay, and, at worst, structural damage to the whole jack-up system. Spudcan-footprint interaction has been identified as the second most common reason for the geotechnical failure of jack-ups [3].

To alleviate this issue, the first step was to investigate the performance of a spudcan installation next to a footprint. Due to both physical testing and numerical simulation challenges, the problem was simplified by considering a single cylindrical leg attached to a flat plate or generic spudcan and either a fixed head condition at the top of the leg [4-10] or a free head condition that allows sliding of the leg [11-13]. The soil failure mechanisms were exposed, the underlying behaviour was elucidated, and the critical offset ratio λ (defined as $\lambda = \beta/D$, where β is the distance between the footprint centre and the spudcan centre, and D is the spudcan diameter) was identified as 0.5~1.

The following step was to explore potential mitigation measures. Thus far a number of measures have been trialled or examined, including: (a) infilling the crater [14,15]; (b) capping the infilled crater with gravel loading platforms; (c) stomping [15,16]; (d) reaming [16-18]; (e) perforation drilling [12]; (f) successive repositioning until the legs stabilise in the desired position [19]; (g) use of a spudcan with a diameter identical or very similar to the existing footprint diameter, placed in the same location as the existing footprint [20]; and (h) simultaneous water jetting and spudcan preloading [21]. In relation to the case histories in the North Sea, Jardine et al. and Grammatikopoulou et al. [15,22] examined the potential of using the former two measures. However, the results were mostly inconclusive or unsatisfactory. The pattern of soil movement became markedly asymmetrical, which led to intolerable forces and moments developing in the jack-up leg before the target preload level was reached. Infilling the crater with different type of soil created additional problems such as punch-through. Use of a gravel loading platform incurred the potential for slope-base failure. Stomping involves raising and lowering the jack-up leg over and away from the footprint to displace the soil towards the footprint. Jardine et al. [15] and Hartono [16] tested stomping and showed that it is effective in mitigating spudcan-footprint interactions where a spudcan penetrated up to the depth of initial penetration during creating the footprint. Reaming, also known as leg-working or leg reciprocation, was tested by Hartono [16] and Hartono et al. [17,18], varying strategies involving different amplitude of leg penetration-extraction cycles. It was found that reaming technique is only effective when a small amplitude of penetration-extraction cycle was used. Perforation drilling involves puncturing the soil by drilling a number of holes (and removing the soil) up to some depths beneath the footprint toe. Hossain & Stainforth [12] showed that the removal of soil inside the spudcan perimeter, with an area of 9% perforated, is effective in easing spudcan-footprint interactions. However, all these techniques require additional mechanical operations to be carried out offshore, leading to additional cost and time.

Consequently, Hossain et al. and Jun et al.[13,23,24] have focused on adjusting spudcan shapes to ease spudcan-footprint interactions. These studies have led to the establishment of a novel spudcan shape with a flat base and 4 holes [24]; the flat base reduces the induced horizontal force on the bottom slope of the spudcan and the holes provide a preferential soil flow path and force the spudcan to penetrate vertically. It has been shown that this shape can effectively ease spudcan-footprint interaction issues such as reducing the induced horizontal force. However, like the previous research on traditional spudcans these studies have considered only a single leg or fixed head condition with a novel spudcan; hence, the results cannot reflect the global behaviour of a jack-up rig, which may undergo leg splay and rotation and is effected by the connecting hull and other two legs.

This study focuses on the effect of global jack-up rig behaviour on spudcan-footprint interactions. The investigation was carried out through 3D large-deformation finite element (LDFE) analyses of soil-structure interaction combining a global jack-up structure idealised by equivalent beam elements. Both leg-by-leg and simultaneous all-leg preloading processes [25], as commonly or sometimes used in the field, are considered with appropriate boundary conditions. An extensive parametric investigation was undertaken, varying the footprint geometry, soil strength and spudcan shape. Finally, the risk of sliding towards the footprint centre, overturning of the jack-up rig and structural failure were assessed by the proposed global jack-up modelling technique.

2. NUMERICAL ANALYSIS

3D LDFE analyses were carried out using the coupled Eulerian-Lagrangian (CEL) approach in the commercial Finite Element (FE) package ABAQUS/Explicit (Version 6.12) [26]. Qiu et al, Chen et al., Tho et al., Hu et al., Hamann et al., Kim and Hossain, Zheng et al. [27-35] have investigated various geotechnical problems using the CEL approach and provided evidence that it is applicable to solve problems involving large deformations. Extensive background information about CEL, spudcan installation and footprint modelling can be found in Jun et al., Zheng et al. and Hu et al. [23,24,35,36]; this information is not repeated here.

2.1 Modelling for spudcan-footprint interaction

Considering the symmetry of the problem, half of the spudcan and soil were modelled. The lateral extension of the soil domain was 4.0D from the centre of the spudcan (D is the spudcan diameter) on the spudcan penetration side and 3.0D on the opposite side, and the depth of the soil domain was ~5.5D to avoid boundary effects during the installation process (as obtained from preliminary convergence studies and considered by researchers [23,35]). Mesh convergence studies were performed to ensure that the mesh was sufficiently fine to give accurate results. Five different mesh densities were considered in the fine mesh zone. The numerical results based on two different minimum element sizes (e.g. h_{min} = 0.021D or 11 elements per hole and h_{min} = 0.025D or 9 elements per hole) were almost identical, indicating that mesh convergence was achieved with the density of h_{min} = 0.025D [23,30]. Therefore, the typical soil element size along the trajectory of the spudcan (i.e., in the fine mesh zone) was selected as 0.025D. A footprint was made using a void. A typical mesh is shown in Fig. 2.

A conical footprint (with diameter, D_F = 2D and depth, z_F = 0.33D; see Fig. 2b) or a cylindrical footprint (with diameter, D_F = D and depth, z_F = 0.66D; see Fig. 2c) with the soil strength along and adjacent to the footprint identical to the intact strength profile was considered. Generally, natural fine grained soils experience remoulding during a spudcan penetration and extraction event. This disturbance is healed gradually with the passing of time through dissipation of excess pore pressure [4,6]. The changes of strength in kaolin clay were presented by Gan et al. [6] plotting strength contour as a function of the jack-up operational period (0 and 2 years) and the intervening period before reinstallation (1 and 100 years). Leung et al. [4] showed a full recovery of the original strength in kaolin takes 1~1.5 years in the vicinity of the footprint. In this study, the soil strength along and adjacent to the footprint identical to the intact strength profile was considered because of two main reasons: (i) removing the variety of possible strength gradients around the footprint has allowed for a consistent evaluation of the benefits of a new global modelling technique (and comparisons with the existing data from centrifuge tests [7] and numerical analyses [15], as reported by Jun et al. [23,24]), (ii) due to the limitation of the current CEL approach and the used Tresca soil model, it is not possible to capture the effect of the jack-up operational period and the intervening period before reinstallation, and to maintain suction at the base of the extracting spudcan [37,38].

This study considered two different spudcan shapes: (a) a generic spudcan with a shape similar to the spudcans of the 'Marathon LeTourneau Design, Class 82-SDC' jack-up rig [39], and (b) a novel spudcan with a flat base and four holes [24] for easing spudcan-footprint interaction issues. The details of these shapes are shown in Fig. 3. These spudcans were simplified as a rigid body and connected to the jack-up rig (this will be discussed later).

The penetration velocity of the spudcan (v) was assumed to be a constant of 0.1 m/s referring the parametric studies [30,40]. Note, with this constant penetration rate, the rapid leg run or uncontrolled leg run cannot be considered. Typically, reinstallation of spudcans in clay is completed under undrained conditions. Furthermore, in practice, natural soils exhibit strain-rate dependency and also softens as they are sheared and remoulded. Thus, the soil was modelled as an elasto-perfectly plastic material that obeys a Tresca yield criterion that was extended to capture the combined effects of rate dependency and progressive softening following Einav and Randolph [41]. The undrained shear strength at individual Gauss points was modified immediately after each step, according to the average rate of shear strain in the previous time step ($\dot{\gamma}$) and the current accumulated absolute plastic shear strain (ξ), as

$$s_u = \left[1 + \mu \log\left(\frac{\mathrm{Max}\left(|\dot{\gamma}|, \dot{\gamma}_{ref}\right)}{\dot{\gamma}_{ref}}\right)\right]\left[\delta_{rem} + \left(1 - \delta_{rem}\right)e^{-3\xi/\xi_{95}}\right]s_{u,ref} \quad (1)$$

The shear strain rate, $\dot{\gamma}$, within the soil was evaluated according to

$$\dot{\gamma} = \frac{\Delta\varepsilon_1 - \Delta\varepsilon_3}{\Delta t} \quad (2)$$

where $\Delta\varepsilon_1$ and $\Delta\varepsilon_3$ are the cumulative major and minor principal strains, respectively, over the incremental time. All the parameter definitions are given in the notation list. Further details can be found in [34,35,42]. The importance of considering this extended soil model, compared to a simple rate-independent and non-softened Tresca model, and corresponding effects have recently been highlighted by spudcan-footprint interaction problems by Zhang et al. [10], Hartono et al. [18], Jun et al. [23,24] and Zhang [43] for other problems by many researchers e.g. Hossain and Randolph [42], Zhou and Randolph [44], Kim et al. [45] and hence not repeated here. The soil-spudcan interface was modelled as frictional contact using a general contact algorithm with a limiting shear stress.

The mesh dependence of the strain softening behavior can be compensated by combining the rate-dependent model (Needleman [46]; Sluys and De Borst [47]; Oka [48]; Zhou and Randolph [44]). For that and for considering at least a reasonable operative shear strength, combined rate dependency and progressive softening was implemented although the considered constant penetration rate of 0.1 m/s may not represent the rate during a spudcan sliding towards a footprint centre. Further accuracy of this numerical model was confirmed by Jun et al. [23,24] through e.g. mesh size exercise and validation exercise against measured centrifuge test data.

2.2 Modelling for a simplified global jack-up rig

To examine the global behaviour induced by spudcan-footprint interactions, a simplified jack-up rig was modelled, as shown in Fig. 2. According to the 'equivalent leg' and 'equivalent hull' model schemes [49], the legs and hull were constructed by 'beam' elements with equivalent properties; the properties of these elements are summarised in Table 1. The hull and legs are generally connected by a jacking system (e.g., roller). In this study, this connection was modelled by 'beam connector' elements, allowing movement in vertical direction (U_z = free) while maintaining the other degrees of freedom (U_x, U_y, R_x, R_y and R_z) fully coupled at the leg-hull connection [15]. The spudcan and a leg were connected by a 'MPC tie' (see Fig. 2), allowing the movement of all degrees of freedom (U_x, U_y, U_z, R_x, R_y and R_z) at the connection point. Symmetric conditions were applied to the overall model. In the field, a hull is generally submerged in shallow water (with a draft) during (at least) the initial preloading, particularly if a hazard (e.g., punch-through or spudcan-footprint interaction) was forecasted. The corresponding vertical buoyancy effect on the hull base was applied using a spring stiffness (K_{buoy}) according to

$$\Delta s = \frac{\Delta F_{buoy}}{K_{buoy}} \tag{2}$$

where Δs is the hull vertical displacement, K_{buoy} (= $\rho_{sea} \times g \times A_{hull\ bottom}$ / number of springs) is the spring stiffness of the static vertical buoyancy effect, and ΔF_{buoy} is the changed static buoyancy force on the hull bottom (or the required force for Δs). ρ_{sea} is the density of the sea water (1.025 ton/m^3), g is the acceleration of gravity (9.81 m/s^2), and $A_{hull\ bottom}$ is the hull base area. Although a controlled leg penetration (0.1 m/s) was modelled, changes of bouncy were occurred due to the rotation of the hull, which was caused by the lateral displacement and rotation of the legs. Note that other environmental loads induced by winds, waves and currents were ignored, as it is usual for a relatively calm weather condition to be considered during preloading [50].

2.3 Modelling for penetration scenarios

To reflect the preloading sequences in the field, two different preloading processes were considered: (a) Preloading A, leg-by-leg preloading: two legs were first installed on the flat ground, and then the third leg was penetrated (at a constant rate of 0.1 m/s) near a footprint (see Fig. 4); (b) Preloading B, simultaneous preloading: all three legs were penetrated simultaneously (at a constant rate of 0.1 m/s; see Fig. 5). To reduce the computational time, the spudcans on the flat ground were replaced by foundation springs. The details of the modelling techniques are described below.

Preloading A, leg-by-leg preloading: The spudcans installed on the flat ground were assumed to be pre-embedded to a depth of 0.25D [8]. The spudcans were replaced by attached foundation springs (see Fig. 4), and the stiffnesses were calculated according to the International Standard Organisation guidelines [51]

$$K_{V,ISO} = K_{dV} \times 2GD / (1-\upsilon) \qquad \text{(vertical stiffness)} \qquad (3)$$

$$K_{H,ISO} = K_{dH} \times 16GD(1-\upsilon) / (7-8\upsilon) \qquad \text{(horizontal stiffness)} \qquad (4)$$

$$K_{M,ISO} = K_{dM} \times GD^3 / 3(1-\upsilon) \qquad \text{(moment stiffness)} \qquad (5)$$

where K_{dV}, K_{dH} and K_{dM} are the stiffness depth factors, G is the shear modulus of the foundation soil and υ is Poisson's ratio of the soil. The third spudcan then penetrated the footprint slope at a constant penetration velocity of v = 0.1 m/s. Note that it was assumed that a single leg penetration is carefully controlled by sequential filling and discharge of preload ballast tanks around the leg to minimise the impact on the global moment equilibrium [50].

Preloading B, simultaneous preloading: All legs are sometimes installed simultaneously, as reported by Amodio et al. [25] for a jack-up rig installation near an existing footprint. They employed simultaneous preloading of three legs in the initial preloading stage (see Fig. 5). The changes in the stiffness of the other two legs during this continuous penetration process cannot be represented by the foundation stiffness from the ISO guidelines [51], which give a constant stiffness at a given depth (Equations 3~5). Therefore, the evolution of stiffness was derived directly from a series of LDFE simulations considering the same soil and spudcan properties. For example, as shown in Fig. 6a, the simplified vertical stiffness ($K_{V,LDFE}$) was extracted from the results of penetration tests on the flat ground. In addition, the simplified horizontal ($K_{H,LDFE}$) and moment ($K_{M,LDFE}$) stiffness were obtained from lateral swipe and rotation tests at different depths (d/D = 0.0, 0.1 and 0.2), respectively (see Fig. 6b and 6c). The correlation of the combined load components was not considered. This modelling approach is consistent with that followed by [52,53] for the study of monopoles and bucket foundations. The penetration velocity (v) of the three legs was assumed to be 0.1 m/s.

3. RESULTS AND DISCUSSION

To examine the effect of various factors on jack-up rig spudcan-footprint interactions, an extensive parametric study was carried out varying the (a) preloading processes (preloading A and preloading B), (b) soil strength ($s_{u,ref}$ = 2.4 + 1.35z kPa to represent soft clays and 50 kPa corresponding to very stiff clays), (c) footprint geometry (D_F = 2D and z_F = 0.33D to represent footprints in soft clays, e.g., [20,54-56]; and D_F = 1D and z_F = 0.66D to represent footprints in moderate to stiff clays, e.g., [57]), and (d) spudcan shape (generic spudcan and novel spudcan; D = 15 m). The results from this parametric study, as assembled in Table 2, are discussed below. The parameters for the rate dependency and strain-softening of the clay soil were assumed to be μ = 0.1, δ_{rem} = 1/S_t = 1/3, ξ_{95} = 15, and $\dot{\gamma}_{ref}$ = 1.5% h^{-1}, as they typically provided a good match with the data from the field and centrifuge tests [23,35].

3.1 Effect of preloading process and foundation stiffness

The effect of the global behaviour of spudcan-footprint interactions was investigated by comparing the modelling results with those from single spudcan penetration analyses with a fixed head condition (infinite horizontal and rotational stiffness, allowing only vertical displacement). The soft clay conditions ($s_{u,ref}$ = 2.4 + 1.35z in the Gulf of Mexico; [39]), conical footprint geometry (D_F = 2D and z_F = 0.33D; see Fig. 2b), and λ = 0.55 were chosen from the field measurements and centrifuge tests. As noted previously, two different preloading processes were considered by using different types of foundation stiffness (K_{ISO} and K_{LDFE}). For simultaneous preloading (preloading B), additional reduction of the foundation stiffness (e.g., $\omega \times K_{LDFE}$, where ω = 0.1, 0.3 and 0.5) was considered to quantify the effect of the foundation stiffness. These reduced stiffness cases correspond to various spudcan embedment conditions and seabed soil strength heterogeneity, for instance, one leg penetrating the footprint slope while the other two legs are adjacent to a region that is lower than the footprint area. A similar approach using reduced stiffness was considered by Kong et al. [8].

Fig. 7 shows a comparison of the performance of the generic spudcan in terms of the horizontal (H), vertical (V), moment (M) stiffnesses, lateral displacement (δ) and rotation distribution (θ) at the spudcan reference point RP (see Fig. 3) along the normalised penetration depth d/D. The corresponding soil failure mechanisms are displayed in Fig. 8. The profiles of the vertical force (V) for the fixed head condition with the two global jack-up rig preloading processes are very consistent (Fig. 7a). However, for preloading B, a reduced stiffness resulted in a reduced vertical resistance at shallow penetration depths (d/D

< 0.2). This is due to sliding with the increasing lateral displacement allowing for a reduction in the resistance (see Fig. 7d). As shown in Fig. 8, during sliding, instead of vertical penetration, the movement of the spudcan along the footprint slope dominates the behaviour. The lateral sliding stops at approximately d/D = 0.2 (the maximum lateral displacement, δ_{max} = 6.23 m for ω = 0.1), where the base of the spudcan is in full contact with the soil (see Fig. 8b); hence, the penetration resistance profile rises sharply and merges with those of the no sliding or minor sliding cases.

The induced horizontal force (H) with global modelling is 8~9% lower than that with the fixed head condition (0.93~0.94MN vs 1.02 MN; see Fig. 7b). This reduction arises mainly from the lateral sliding towards the footprint centre, diminishing the asymmetry of the soil failure mechanism (see Figs. 7d and 8). Relative to the fixed head condition, both reduction of H and lateral sliding displacement δ increase with decreasing stiffness K (Figs. 7b and 7d) confirms the previously identified explanation. The maximum horizontal force (H_{max}) for $0.1 \times K_{LDFE}$ is 0.25 MN, which is approximately 75% lower than that for the fixed head condition (H_{max} = 1.02 MN).

All the moments (M) in this parametric study are shown in Fig. 7c. The moment (M) at RP is mainly governed by the resultant vertical force (V) and its eccentricity from RP as the resultant horizontal forces nearly pass through RP [7,10,23-24]. As such, the differences in the maximum moment (M_{max}) are not very large (see Fig. 7c).

The lateral displacement, δ, and rotation, θ, are plotted in Fig. 7d and 7e, respectively. Both values are 0 regardless of the penetration depth for the fixed head condition, as the spudcan was forced to penetrate vertically. The maximum lateral displacements for preloading A and preloading B are respectively δ_{max} = 0.49 m and 0.55 m, which increase with decreasing ω or stiffness (Fig. 7d). For instance, δ_{max} = 6.23 m for $\omega = 0.1$. Interestingly, the trend is reversed for the rotation θ. The maximum rotation value θ_{max} is -0.23° for preloading A and

-0.13° for preloading B. θ_{max} decreases with ω or the stiffness (Fig. 7e). For instance, θ_{max} = -0.04° for ω = 0.1. This is because of the domination of the global jack-up movement mechanism, translational to leg splay, as explained below.

Fig. 9 shows the schematic diagram for the relative lateral displacement (δ) and rotation (θ) at four characteristic locations in the jack-up rig: (a) location A ($\Delta\delta_a$ and $\Delta\theta_a$) is at the spudcan on the flat seabed; (b) locations B and C ($\Delta\delta_b$, $\Delta\delta_c$ and $\Delta\theta_b$, $\Delta\theta_c$) are at the connection between the hull and the leg; and (c) location D ($\Delta\delta_d$ and $\Delta\theta_d$) is at the spudcan near the footprint. The values of δ and θ for these four locations from the abovementioned analyses are summarised in Table 3 (note, Fig. 7d and 7e show the resultant lateral displacement ($\delta = \Delta\delta_a + \Delta\delta_b + \Delta\delta_c + \Delta\delta_d$) and rotation ($\theta = \Delta\theta_a + \Delta\theta_b + \Delta\theta_c + \Delta\theta_d$), respectively, at location D). For the relatively higher stiffness cases (i.e., K_{ISO} and K_{LDFE}), the maximum lateral displacements occur at locations B and D, while the displacements at location A and C are minimal. This is because, for instance, at location A, the actual lateral responses lie in the elastic zone of stiffness K_{ISO} and K_{LDFE} (see Fig. 10). This minimum lateral displacement at locations A and C and maximum lateral displacement at B and D results in leg splay of the global jack-up. However, by reducing the foundation stiffness ($\omega \times K_{LDFE}$, ω = 0.1, 0.3 and 0.5), the displacements at location A increase remarkably (see Fig. 10), while those at B and D decrease. Therefore, the global jack-up deformation pattern changes to a horizontal translational mode (see insets in Fig. 10).

In all the cases, the rotation increments at location D ($\Delta\theta_d$) are almost identical to the resultant rotation at the spudcan location RP (θ; see Table 3). This attributes to the fact that the buoyancy spring stiffness (K_{buoy}) restricts the rotation of the hull, leading to the other rotation components compensating with each other ($\Delta\theta_a + \Delta\theta_b + \Delta\theta_c \approx 0$).

3.2 Evaluate structural integrity

With the global jack-up modelling technique, the structural integrity of the jack-up leg can be assessed. To generate a large horizontal force (and hence the leg failure load) from the spudcan-footprint interaction, a very stiff clay ($s_{u,ref}$ = 50 kPa) and corresponding foundation stiffness (e.g., K_{ISO}) were considered as pre-embedded conditions for the spudcan on the flat ground. According to the centrifuge tests reported by Gan [54], a cylindrical footprint geometry (D_F = 1.00D and z_F = 0.66D; typical footprint geometry in stiff clay; see Fig. 2c) and λ = 0.5 were selected.

The spudcan responses and corresponding failure mechanisms from the global jack-up modelling are presented in Fig. 11 and 12, respectively. The results from a single spudcan penetration with a fixed head condition are also included in Fig. 11 for comparison. Consistent with Fig. 7, the global responses (vertical load, horizontal load and moment in Fig. 11) are lower than the fixed head responses. However, as expected, the lateral displacement and rotation are greater for the global jack-up.

By comparing with the results in Fig. 7, all the spudcan responses for a deep cylindrical footprint in stiff clay are significantly higher than the corresponding results for a shallow conical footprint in soft clay, although the offsets of the spudcan penetration are very similar, λ = 0.5 (Fig. 11) and 0.55 (Fig. 7). For instance, the maximum horizontal force (H_{max}) is 682% greater for a deep cylindrical footprint. This is because of the more profound asymmetric soil flow to deeper penetration depths, as can be observed by comparing the soil failure mechanisms between Fig. 8 and 12, and the increased undrained shear strength. In addition, the global modelling confirms that the lateral sliding towards the footprint centre reduces the induced horizontal force.

Fig. 7c and 11c plot the moment at RP at the spudcan centre, nominally nulling the influence of the resultant horizontal force H, as it nearly passes through the RP. However, if the reference point is shifted to the point connecting the leg with the hull, the resultant horizontal force H will add additional moment (= H × L_{leg}) and dominate the moment response [23,24]. If the consequent stress on the leg exceeds its structural capacity, the leg can be damaged. For example, Fig. 13a plots the moment at the leg top for the preloading A (K_{ISO}) case shown in Fig. 11c. Clearly, the moment direction is reversed, and the magnitude of the maximum moment is significantly higher (-467.5 MN vs 72 MN). Fig. 13b shows that the beam stress distribution on the leg interacts with the footprint just below the hull (150 m above the soil surface), which is captured directly from the global jack-up modelling. The beam stress can be divided into two components: (a) pure axial stress from the vertical force (e.g., penetration resistance) and (b) bending stress from the spudcan-footprint interaction (i.e., horizontal force, moment, leg eccentricity; see inset in Fig. 13b). In this case, the structural stability of the leg is dictated by the bending stress due to the effect of the spudcan-footprint interaction. For instance, when the maximum beam stress ($\sigma_{beam,max}$) is approximately -420.8 MPa, the axial stress (σ_{axial}) is -82.2 MPa (19.5% of σ_{beam}) and the bending stress ($\sigma_{bending}$) is -338.6 MPa (80.5% of σ_{beam}). Fig. 13c shows the evolution of structural stresses with the spudcan penetration depth d/D, allowing the identification of the critical depth for attaining the maximum beam stress as $d/D_{critical}$ = 0.45.

In the analyses above, the jack-up legs were simplified according to the ‘equivalent leg’ model scheme of SNAME [49]. To assess the structural integrity more precisely, an analysis was performed by considering a truss leg, following the ISO design guideline [51]. From the analyses above(e.g., Fig. 13), it was found that the maximum stress was concentrated on the leg with the spudcan to be installed near the footprint, just beneath the connection of the hull with the leg. As such, for this analysis, only a 37.5-m-long section of that leg from the hull-leg connection point was considered, as shown in Fig. 14. For the boundary conditions, three degrees of freedom (lateral displacement in the x direction, U_x, vertical displacement,

U_z, and rotation in the y direction, R_y) at the top and bottom of the truss leg section were considered, while lateral displacement in the y direction (or perpendicular to the page), U_y, rotation in the x direction, R_x, and rotation in the vertical direction, R_z, were assumed to be zero due to the symmetric condition of the problem.

In ISO guidance [51], the structural stability requirement for the chord is suggested to be

$$|\sigma_{beam,max}| < \sigma_{criteria} \tag{6}$$

where $\sigma_{criteria} = \sigma_{column\ buckling} / F_{safety}$

$$\sigma_{column\ buckling} = (1.0 - 0.278 \times \chi^2) \times \sigma_{yield} \qquad \text{for } \lambda \leq 1.34$$

$$= 0.9 \times \sigma_{yield} / \chi^2 \qquad \text{for } \lambda > 1.34$$

F_{safety} = resistance factor = 1.15

$\chi = (\sigma_{yield} / \sigma_E)^{0.5}$

σ_E = Euler buckling strength = $\pi^2 E_{steel} / (K \times L_{bay} / r_{r\&c})^2$

K = column effective length factor = 1.0

The yield strength (σ_{yield}) for the chord typically ranges from 414 to 700 MPa depending on the jack-up rig size and type [51]. L_{bay} is one bay length, $r_{r\&c}$ is the radius of gyration of the rack and chord, and E_{steel} is Young's modulus of the steel. The considered dimensions and properties of the chord and brace are summarised in Table 4. According to Equation 6, $\sigma_{criteria}$ varies between 302.8 and 445.3 MPa.

Fig. 15 shows the results in terms of beam stresses in the leg. The maximum stress (-398.8 MPa) occurs at the second (from the top) joint between the left chord and braces (see the zoomed-in figure of the left chord in Fig. 15). The maximum absolute value of the beam stress at the joint, $|\sigma_{beam,max}|$ = 398.8 MPa, exceeds the lower bound of the design criteria, 302.8 MPa < $\sigma_{criteria}$ < 445.3 MPa (calculated with Equation 6 and the input from Table 4).

Therefore, $|\sigma_{beam,max}| > \sigma_{criteria}$, indicating that leg failure may occur if a leg of the jack-up rig is installed on a deep cylindrical footprint in very stiff clay.

Interestingly, the maximum absolute beam stress from the global modelling with simplified legs (-420.8 MPa in Fig. 13) closely predicts (just 5.5% higher) the maximum stress from the detailed truss leg analysis (398.8 MPa in Fig. 15). Although simplified leg modelling cannot indicate the exact location of the likelihood of failure on the global jack-up structure, a critical zone can be identified. Note that if the maximum absolute stress from the global modelling with simplified legs (σ_{beam}) is close to or exceeds the stability criterion ($\sigma_{criteria}$), a detailed truss leg analysis has to be conducted.

3.3 Effect of novel spudcan

From the previous investigations [13,23,24], it has been consistently found that spudcan shape has a significant influence on spudcan-footprint interactions, leading to the establishment of a novel spudcan shape, with a flat base and 4 holes, to ease spudcan-footprint interaction issues. For example, the reduction of the maximum induced horizontal force (H_{max}) by the novel spudcan was approximately 30%~42% [24] and the reduction of the lateral sliding distance was 74~98% [13], in comparison to the results using a generic spudcan. However, all the previous simulations or tests have been conducted considering a single rigid leg with either a fixed head or free head (allowing lateral displacement of the spudcan and leg together [13]) condition. In this study, the performance of the novel spudcan will be assessed through global jack-up rig modelling.

Lateral sliding

To check the effect of the novel spudcan on lateral sliding, a normal (preloading B; K_{LDFE}) and a reduced (preloading B; $0.1 \times K_{LDFE}$) foundation stiffness and a conical shallow footprint geometry ($D_F = 2D$ and $z_F = 0.33D$), were chosen. Fig. 16 shows the response profiles for both novel and generic spudcans as comparison. For the normal stiffness case, the novel spudcan reduces H_{max} by 31% and θ_{max} by 23%, but the values of M_{max} (near RP) and δ_{max} are very similar. In contrast, for the reduced stiffness case, the values of H_{max}, M_{max} and θ_{max} are similar, but the novel spudcan reduces δ_{max} by 40%. These results can be explained by the corresponding soil failure mechanisms depicted in Fig. 17. By comparing the mechanisms for the generic spudcan in Fig. 8, the flat-based underside profile and holes on the novel spudcan provide preferential soil flow paths, somewhat anchoring the spudcan on the right slide with earlier soil flow through the holes and forcing the spudcan to penetrate more vertically, reducing H_{max} (for the normal stiffness case) or θ_{max} (for the reduced stiffness case).

Note that the vertical resistance of the novel spudcan is lower than that of the generic spudcan up to d/D = ~0.25 due to the reduced net area (A_{net} = 141.4 m^2 for the novel spudcan vs 176.7 m^2 for the generic spudcan). Therefore, to confirm the mitigation efficiency of the novel spudcan shape, an additional analysis was carried out on a large novel spudcan of D = 16.4 m (with A_{net} equal to the generic spudcan). Here, only the flat base part was increased to get an identical A_{net} (see inset in Figure 16). As expected, (i) the vertical force for the large novel spudcan (D = 16.4 m) becomes similar to the generic spudcan (Figure 16a), (ii) the horizontal force remains similar to the original novel spudcan (Figure 16b) as the enlarged flat base did not mobilise additional horizontal force, and (iii) the moment response increases significantly due to the enhanced imbalance vertical force (Figure 16c). The effect of the holes has been reported extensively by Jun et al. [23, 24].

Leg failure

To examine the effect of the novel spudcan on the structural integrity, stiff clay with a deeper footprint case, discussed in Fig. 11~15, was considered. The same analyses were carried out by replacing the generic spudcan with the novel spudcan. The results are shown in Fig. 18~20.

Compared to the response of the generic spudcan, the maximum horizontal force (H_{max}), maximum moment (M_{max}), maximum lateral displacement (δ_{max}), and maximum rotation (θ_{max}) are reduced by 34.2%, 19.2%, 31.5% and 22.6%, respectively, by using the novel spudcan (see Fig. 18). With the progress of penetration, the soil flow beneath the generic spudcan is mainly directed towards the other side of the footprint wall (see Fig. 12a and b), whereas the soil at the base of the novel spudcan flows partly through the holes and partly towards the other side of the footprint wall (see Fig. 19a and b). The soil flow through the holes somewhat anchors the spudcan, limiting the lateral sliding of the spudcan towards the footprint centre.

Fig. 20a shows the stress distributions, as a function of the normalised spudcan penetration depth d/D, from the global modelling considering simplified beam legs. The critical spudcan penetration depth for attaining the maximum stress, $d/D_{critical} = 0.5$, is similar to that (0.45) for the generic spudcan (see Fig. 13c). However, the maximum beam stress of $\sigma_{beam,max} = -315.9$ MPa is 25% lower than that (420.8 MPa) for the generic spudcan. Nevertheless, $|\sigma_{beam,max}| = 315.9$ MPa exceeds the lower bound of the design criteria, 302.8 MPa < $\sigma_{criteria}$ < 445.3 MPa. As such, a detailed truss leg analysis was carried out, and the stress distribution is shown in Fig. 20b. Again, the location of the maximum beam stress at the 2nd (from the top) joint between the left chord and braces is consistent with the location of the maximum beam stress for the generic spudcan (see Fig. 15). However, the maximum beam stress of $|\sigma_{beam,max}| = 298.6$ MPa is now less than the lower bound of the design criteria, 302.8 MPa < $\sigma_{criteria}$ < 445.3 MPa, meaning that the leg or jack-up rig will not fail if the novel spudcan is used. This confirms that tweaking the spudcan shapes (i.e., the underside profile and holes) has potential to ease spudcan-footprint interactions and increases the structural integrity of the jack-up rig.

4. CONCLUDING REMARKS

A global assessment of spudcan-footprint interactions was performed through modelling of a complete jack-up rig considering three simplified tubular legs connected by a hull than that performed using a single leg or fixed head condition. The influence of buoyancy on the hull draft was taken into account. The two routine preloading methods, i.e. leg-by-leg preloading and simultaneous preloading, were simulated. The jack-up rig was set up with one leg with its spudcan foundation near a footprint and the other two legs with their spudcans away from the footprint. The two spudcans away from the footprint were replaced by vertical horizontal and moment springs to simplify the analysis. The stiffness of the springs were obtained from the LDFE analyses and artificially reduced (to capture softer soil or surface footing case) the values. In addition, two soil strengths and two footprint geometries were explored. Advanced structural integrity analyses were carried out by considering global modelling with a tubular leg or truss leg to identify the potential and location of leg failure due to spudcan-footprint interactions. Finally, the performance of a recently proposed novel spudcan in the global jack-up rig was assessed. The following conclusions can be drawn.

Global jack-up rig modelling showed that induced horizontal force H_{max} may be 8~9% (for soft clay with a 2D wide and 0.33D deep footprint) and 15.9% (for stiff clay with a 1D wide and 0.66D deep footprint) lower compared to the fixed head condition. However, this study also provided an indication of the magnitude of the lateral spudcan displacement, with maximum displacements of δ_{max} = 0.45~0.55 m (for soft clay) to 3.43 m (for stiff clay), and maximum rotations of θ_{max} = -0.13~-0.23° (for soft clay) and -1.37° (for stiff clay). The reduction of H with global modelling increased with decreasing stiffness K and increasing lateral sliding displacement δ. The effect of preloading process was found to be insignificant. All the responses for a deep cylindrical footprint in stiff clay were significantly higher compared to the results for a shallow conical footprint in soft clay, with identical spudcan installation offset.

For the stiff clay with a 0.66D deep footprint and generic spudcan, the maximum beam stress occurred at a spudcan penetration depth of 0.5D. Both the global analysis with a tubular leg and detailed truss leg analysis showed that the leg on the footprint would fail at the second (from the top) joint between the left chord and braces due to the beam stresses caused by spudcan-footprint interactions.

The novel spudcan with a flat base and 4 holes reduced H_{max} by 31% and θ_{max} by 23% (for soft clay with a 2D wide and 0.33D deep footprint) and H_{max} by 34.2%, δ_{max} by 19.2% and θ_{max} by 31.5% (for stiff clay with a 1D wide and 0.66D deep footprint) against the generic spudcan. More importantly for the cases studied here, from the detail truss leg analysis, the leg near the footprint, which would fail with the generic spudcan, may not fail with the novel spudcan.

Based on the results, the recommendations for the design of a spudcan penetration near a footprint can be proposed as

1. The responses are affected by the footprint geometry, offset distances, and spudcan shape.
2. To prevent the large lateral displacement towards the footprint centre, the horizontal resistance capacity at the other spudcans should be larger than the horizontal force induced by spudcan-footprint interactions.
3. The structural integrity of the leg must be checked against the predicted induced horizontal force and moment.

4. The novel spudcan can be used for easing spudcan-footprint interactions.

All the analyses were performed considering a footprint with the soil strength along and adjacent to the footprint identical to the intact strength profile. The changes of soil strength during the formation of the footprint and subsequent jack-up operational period and the intervening period before reinstallation was therefore not taken into account. Further analyses are being carried out considering soil strength heterogeneity around the footprint. Due to the limitation of the used LDFE technique and soil constitutive model, footprint was not created in the real field way of penetration and extraction of a spudcan. Instead, the footprint geometries and strength contour presented by Gan et al. [6] as a function of the jack-up operational period and the intervening period before reinstallation were directly mapped in the LDFE simulations. The results will be published in the future.

5. ACKNOWLEDGEMENTS

The research presented herein was undertaken with support from the Australian Research Council (ARC) through Linkage Project LP140100066. The work forms part of the activities of the Centre for Offshore Foundation Systems (COFS), currently supported as a node of the Australian Research Council Centre of Excellence for Geotechnical Science and Engineering and as a Centre of Excellence by the Lloyd's Register Foundation. This support is gratefully acknowledged, as is the helpful discussion with Dr. Dong Wang.

REFERENCES

[1] CLAROM. Design guides for offshore structures. Club des Actions de Recherche sur les Ouvrages en Mer, Eds: Le Tirant, P. & Pérol, C., Paris; 1993.

[2] Randolph MF, Cassidy MJ, Gourvenec S, Erbrich CJ. (2005). Challenges of offshore geotechnical engineering. State of the art paper, Proc Int Conf on Soil Mech and Found Eng; 2005 Sep 12-15; Osaka, Japan. 2005. 1:123–76.

[3] MSL Engineering Limited for the Health and Safety Executive. Guidelines for jack-up rigs with particular reference to foundation integrity; 2004. Research Report 289.

[4] Leung CF, Gan CT, Chow YK. Shear strength changes within jack-up spudcan footprints. Proc 17th Int Offshore and Polar Eng (ISOPE); 2007 Jul 1-6; Lisbon, Portugal. 2007. 2:1504-09.

[5] Cassidy MJ, Quah CK, Foo KS. Experimental investigation of the reinstallation of spudcan footings close to exiting footprints. J Geotech Geoenviron Eng (ASCE) 2009;135(4):474–86.

[6] Gan CT, Leung CF, Cassidy MJ, Gaudin C, Chow YK. Effect of time on spudcan-footprint interaction in clay. Géotechnique 2012;62(5):401–13.

[7] Kong VW, Cassidy MJ, Gaudin C. Experimental study of the effect of geometry on reinstallation of jack-up next to footprint. Canadian Geotech J 2013;50(5):557-73.

[8] Kong VW, Cassidy MJ, Gaudin C. Development of a real-time hybrid testing method in a centrifuge. Int J Phys Modelling in Geotech 2015;15(4):169-90.

[9] Tho KK, Leung CF, Chow YK, Swaddiwudhipong S. Eulerian finite-element simulation of spudcan-pile interaction. Canadian Geotech J 2013;50(6):595-608.

[10] Zhang W, Cassidy MJ, Tian Y. 3D large deformation finite element analyses o jack-up reinstallations near idealised footprints. Proc 15th Int Conf on the Jack-up Platf: Design, Construction and Operation; 2015 Sep15-16; City University London, UK. 2015.

[11] Gaudin C, Cassidy MJ, Donovan T. Spudcan reinstallation near existing footprints. Proc Offshore Site Investigation and Geotech Conf, Confronting New Challenges and Sharing Knowledge; 2007 Sep 11-13; London, UK. 2007. p. 285-92.

[12] Hossain MS, Stainforth R. Perforation drilling for easing spudcan-footprint interaction issues. Ocean Eng 2016;113:308-18.

[13] Hossain MS, Stainforth R, Ngo VT, Cassidy MJ, Kim YH, Jun MJ. Experimental investigation on the effect of spudcan shape on spudcan-footprint interaction. Appl Ocean Res 2017;69:65-75.

[14] Jardine RJ, Kovecevic N, Hoyle MJR, Sidhu HK, Letty A. A study of eccentric jack-up penetration into infilled footprint craters. Proc 8th Int Conf on the Jack-up Platf: Design, Construction and Operation; 2001 Sep 18-19; City University London, UK. 2001.

[15] Jardine RJ, Kovacevic N, Hoyle MJR, Sidhu HK, Letty A. Assessing the effects on jack-up structures of eccentric installation over infilled craters. Proc Offshore Site Invest and Geotech Conf, Diversity and Sustainability; 2002 Nov 26-28; London, UK. 2002. p. 307–24.

[16] Hartono. Centrifuge model study on spudcan-footprint remediation techniques. Ph.D. thesis, National University of Singapore, 2014.

[17] Hartono, Leung DF, Tho KK, Chow YK. Reaming as mitigation measure for jack-up reinstallation close to existing footprint. Proc 14th Int Conf on the Jack-up Platf: Design, Construction and Operation; 2013 Sep 17-18; City University London, UK. 2013.

[18] Hartono, Tho KK, Leung DF, Chow YK. Centrifuge and numerical modelling of reaming as mitigation measure for spudcan-footprint interaction. Offshore Technol Conf (OTC) Asia; 2014 Mar 25-28; Kuala Lumpur, Malaysia. 2014. OTC 024835MS.

[19] Brennan R, Diana H, Stonor RWP, Hoyle MJR, Cheng C-P, Martin D, et al. Installing jackups in punch-through-sensitive clays. Proc Offshore Technol Conf (OTC); 2006 May 1-4; Houston, USA. 2006. OTC 18268.

[20] Erbrich CT, Amodio A, Krisdani H, Lam SY, Xu X, Tho KK. Re-visiting Yolla- new insight on spudcan penetration. Proc 15th Int Conf on the Jack-up Platf: Design, Construction and Operation; 2015 Sep15-16; City University London, UK. 2015.

[21] Handidjaja P, Gan CT, Leung CF, Chow YK. Jack-up foundation performance over spudcan footprints analysis of a case history. Proc 12th Int Conf on the Jack-up Platf: Design, Construction and Operation; 2009 Sep 15-16; City University London, UK. 2009.

[22] Grammatikopoulou A, Jardine RJ, Kovacevic N, Potts DM, Hoyle MJR, Hampson KM. Potential solutions to the problem of the eccentric installation of jack-up structures into old footprint craters. Proc Offshore Site Invest and Geotech Conf, Confronting New Challenges and Sharing Knowledge; 2007 Sep 11-13; London, UK. 2007. p. 293-300.

[23] Jun MJ, Kim YH, Hossain MS, Cassidy MJ, Hu Y, Sim JU. Numerical investigation of novel spudcan shapes for easing spudcan-footprint interactions. J Geotech Geoenviron Eng (ASCE) 2018;144(9):04018055.

[24] Jun MJ, Kim YH, Hossain MS, Cassidy MJ, Hu Y, Park SG. Optimising spudcan shape for mitigating spudcan-footprint interaction. Appl Ocean Res 2018;79:62-73.

[25] Amodio A, Erbrich C, Murugavel V. Re-visiting Yolla – managing jack-up storm stability; geotechnical assessment. Proc 15th Int Conf on the Jack-up Platf: Design, Construction and Operation; 2015 Sep15-16; City University London, UK. 2015.

[26] Dassault Systemes. ABAQUS , Version 6.11 EF Documentation. Rhode Island: Hibbitt, Karlsson and Sorensen, Inc.; 2012.

[27] Qiu G, Henke S, Grabe J. Application of a coupled Eulerian–Lagrangian approach on geomechanical problems involving large deformations. Computer Geotech 2011;38:30-9.

[28] Chen Z, Tho KK, Leung CF, Chow YK. Influence of overburden pressure and soil rigidity on uplift behavior of square plate anchor in uniform clay. Computer Geotech 2013;52:71-81.

[29] Tho KK, Chan N, Zhou Y, Liu J, Zhou S. Case study of spudcan re-penetration analysis using large deformation finite element approach. Proc 15th Int Conf on the Jack-up Platf: Design, Construction and Operation; 2015 Sep15-16; City University London, UK. 2015.

[30] Hu P, Wang D, Cassidy MJ, Stanier SA. Predicting the resistance profile of a spudcan penetrating sand overlying clay. Canadian Geotech J 2014;51(10):1151-64.

[31] Hamann T, Qiu G, Grabe J. Application of a Coupled Eulerian-Lagrangian approach on pile installation problems under partially drained conditions. Computer Geotech 2015;63:279-90.

[32] Kim YH, Hossain MS. Dynamic installation of OMNI-Max anchors in clay: Numerical Analysis. Géotechnique 2015;65(12):1029-37.

[33] Kim YH, Hossain MS. Numerical study on pull-out capacity of torpedo anchors in clay. Géotechnique Letters 2016;6(4):275-82.

[34] Kim YH, Hossain MS. Dynamic installation, keying and diving of OMNI-Max anchors in clay. Géotechnique 2017;67(1):78-85.

[35] Zheng J, Hossain MS, Wang D. New design approach for spudcan penetration in nonuniform clay with an interbedded stiff layer. J Geotech Geoenviron Eng (ASCE) 2015;141(4):04015003.

[36] Hu P, Wang D, Stanier SA, Cassidy MJ. Assessing the punch-through hazard of a spudcan on sand overlying clay. Géotechnique 2015;65(11):883-96.

[37] Z.Chen, K.K. Tho, C.F. Leung, Y.K. Chow, Influence of overburden pressure and soil rigidity on uplift behavior of square plate anchor in uniform clay, Computers and Geotechnics 2013, 52:71-81.

[38] K.K. Tho, Z.Chen, C.F. Leung, Y.K. Chow, Pullout behaviour of plate anchor in clay with linearly increasing strength, Canadian Geotechnical Journal 2014, 51(1):92-102.

[39] Menzies D, Roper R. Comparison of jackup rig spudcan penetration methods in clay. roc Offshore Technol Conf (OTC); 2008 May 5-8; Houston, USA. 2008. OTC 19545.

[40] Wang D, Bienen B, Nazem M, Tian Y, Zheng J, Pucker T, et al. Large deformation finite element analyses in geotechnical engineering. Computer Geotech 2015;65:104-14.

[41] Einav I, Randolph MF. Combining upper bound and strain path methods for evaluating penetration resistance. Int J Numerical Methods Eng 2005;63(14):1991-2016.

[42] Hossain MS, Randolph MF. Effect of strain rate and strain softening on the penetration resistance of spudcan foundations on clay. Int J Geomech (ASCE) 2009;9(3):122-32.

[43] Zhang W. Investigation of spudcan-footprint interaction in clay with a novel implementation of a three-dimensional large deformation finite element method. Ph.D. thesis, The University of Western Australia, 2018.

[44] Zhou H, Randolph MF. Computational techniques and shear band development for cylindrical and spherical penetrometers in strain-softening clay. Int J Geomechanics 2007;7(4):287-295.

[45] Kim YH, Hossain MS, Wang D. Effect of strain rate and strain softening on embedment depth of a torpedo anchor in clay, Ocean Eng 2015;108:704-715.

[46] Needleman A. Material rate dependence and mesh sensitivity in localization problems. Comput Methods Appl Mech Eng 1988;67(1):69–85.

[47] Sluys LJ, De Borst R. Wave propagation and localization in a rate-dependent cracked medium-model formulation and onedimensional examples. Int J Solids Struct 1992;29(23):2945–2958.

[48] Oka F. Computational modeling of large deformations and the failure of geomaterials. Proc., 16th Int. Conf. on Soil Mechanics and Foundation Engineering; 2005 Sept12-15; Osaka, Japan. 2005;1:47–94.

[49] Society of Naval Architects and Marine Engineers (SNAME), Site specific assessment of mobile jack-up units. SNAME Technical and Research Bulletin 5-5A. 1st ed. 3rd revision; 2008.

[50] InSafeJIP. Improved guidelines for the prediction of geotechnical performance of spudcan foundations during installation and removal of jack-up units. Joint Industry Funded Project; 2011.

[51] International Organization for Standardization (ISO). Petroleum natural gas industries – Site specific assessment of mobile offshore units – Part 1: Jack-ups; 2012. ISO 19905-1

[52] Ibsen LB, Roesen HR, Wolf TK, Hansen M, Rasmussen KL. Assessment of p-y curves from numerical methods for a non-slender monopile in cohesionless soil. Proc 23rd Int Offshore and Polar Eng (ISOPE); 2013 Jun 30- Jul 4; Alaska, USA. 2013. 2:436-43.

[53] Østergaard MU, Knudsen BS, Ibsen LB. P–y curves for bucket foundations in sand using finite element modelling. Proc 3rd Int Symp on Frontiers in Offshore Geotech (ISFOG); 2015 Jun 10-12; Oslo, Norway. 2015. 1:343-8.

[54] Gan CT. Centrifuge model study on spudcan-footprint interaction [dissertation]. Singapore: National University of Singapore; 2009.

[55] Hossain MS, Dong D, Gaudin C, Kong VW. Skirted spudcans and perforation drilling for installation of spudcans close to existing footprints. Proc Offshore Site Invest and Geotech Conf, Integrated Geotechnologies- Present and Future; 2012 Sep 12-14; London, UK. 2012. p. 597-605.

[56] Hossain MS, Dong X. Extraction of spudcan foundations in single and multilayer soils. J Geotech Geoenviron Eng (ASCE) 2014;140(1):70-184.

[57] Erbrich CT. Australian frontiers – spudcans on the edge. Proc 1st Int Symp on Frontiers in Offshore Geotech (ISFOG); 2005 Sep 19-21; Perth, Australia. 2005. p. 49-75.

Nomenclature

A_{hull}	cross-sectional area of equivalent hull beam model
$A_{hull\ bottom}$	bottom area of jack-up rig hull
A_{leg}	cross-sectional area of equivalent leg beam model
A_{net}	net area of spudcan at largest section
$A_{r\&c}$	cross-sectional area of rack and chord
D	spudcan diameter at largest section
D_{brace}	brace diameter
D_{chord}	chord diameter
D_F	footprint diameter
d	penetration depth of spudcan base
$d/D_{critical}$	normalised critical penetration depth
d_h	hole diameter
E_{steel}	Young's modulus of steel
e_{leg}	eccentricity of leg
G	shear modulus of foundation soil
g	acceleration of gravity
H	horizontal force at spudcan base level
H_{max}	maximum horizontal force at spudcan base level
I_{hull}	moment of inertia of equivalent hull beam model
I_{leg}	moment of inertia of equivalent leg beam model
$I_{r\&c}$	moment of inertia of rack and chord
K	column effective length factor
K_{buoy}	spring stiffness of buoyancy
K_{dV}, K_{dH} and K_{dM}	vertical, horizontal and moment foundation stiffness depth factors
K_{ISO}	foundation stiffness calculated by ISO guidance (2012)
$K_{V,ISO}$, $K_{H,\ ISO}$ and $K_{M,ISO}$	vertical, horizontal and moment foundation stiffness calculated by ISO guidance (2012)
K_{LDFE}	foundation stiffness calculated by LDFE analysis
$K_{V,\ LDFE}$, $K_{H,\ LDFE}$ and $K_{M,\ LDFE}$	vertical, horizontal and moment foundation stiffness calculated by LDFE analysis
L_{bay}	bay length

L_{leg}	length of leg
L_{rack}	length of rack
M	moment at spudcan base level
M_{max}	maximum moment at spudcan base level
M_t	moment at leg top
RP	reference point that is the intersection point of the centre line and largest cross section of the spudcan (see Fig. 3)
R_x, R_y & R_z	rotational displacement
$r_{r\&c}$	radius of gyration of rack and chord
S_t	soil sensitivity
s_u	undrained shear strength
$s_{u,ref}$	reference undrained shear strength
t_{brace}	brace thickness
t_{chord}	chord thickness
t_{rack}	rack thickness
U_x, U_y & U_z	directional displacement
V	vertical force
v	spudcan penetration velocity
z	penetration depth below soil surface
z_F	footprint depth
α_b	spudcan base angle
β	distance between the footprint centre and spudcan centre
$\Delta F_{buoy.}$	change in static buoyancy force on the hull bottom (or the required force for Δs)
Δs	change in hull vertical displacement
$\Delta\delta_a$, $\Delta\delta_b$, $\Delta\delta_c$, $\Delta\delta_d$	relative deflection at four different locations (see Fig. 9)
$\Delta\theta_a$, $\Delta\theta_b$, $\Delta\theta_c$, $\Delta\theta_d$	relative rotation at four different locations (see Fig. 9)
δ	spudcan lateral displacement at RP
δ_{max}	maximum spudcan lateral displacement
δ_{rem}	remoulded strength ratio
$\dot{\gamma}$	shear strain rate
$\dot{\gamma}_{ref}$	reference shear strain rate

λ	the ratio of the distance between the footprint centre and spudcan centre, β, and the spudcan diameter
μ	rate parameter for logarithmic expression
θ	spudcan rotation at RP
θ_{max}	maximum rotation at RP
ρ_{sea}	density of sea water
σ_{axial}	structural axial stress
σ_{beam}	structural beam stress
$\sigma_{beam,max}$	maximum structural beam stress
$\sigma_{bending}$	structural bending stress
σ_{E}	Euler's buckling strength
$\sigma_{criteria}$	design criteria (ISO, 2012)
σ_{yield}	yield stress of steel
υ	Poisson's ratio of foundation soil
ω	reduction factor of foundation stiffness
ξ	cumulative plastic shear strain
ξ_{95}	cumulative plastic shear strain required for 95% remoulding

Table 1. Main dimensions and properties of a simplified jack-up rig model

Main dimensions and properties	Value
Total leg length	180 (m)
Leg length between hull and seabed	150 (m)
Each side length of hull (hull shape: equilateral triangle)	80 (m)
Cross-sectional area of equivalent leg beam model, A_{leg}	0.71 (m^2)
	0.35 (m^2) for a symmetric condition
Cross-sectional area of equivalent hull beam model, A_{hull}	2.79 (m^2)
	1.40 (m^2) for a symmetric condition
Moment of inertia of equivalent leg beam model, I_{leg}	21.26 (m^4)
	10.63 (m^4) for a symmetric condition
Moment of inertia of equivalent hull beam model, I_{hull}	55.51 (m^4)
	27.76 (m^4) for a symmetric condition

Table 2. Summary of 3D LDFE analyses performed

Group	Spudcan shape	$s_{u,ref}$ (kPa)	Footprint depth, z_F (m)	Footprint diameter, D_F (m)	Offset distance, β (m)	Penetration scenario		Spudcan response: H_{max} (MN)	M_{max} (MN-m)	δ_{max} (m)	θ_{max} (°)	Note
I	Generic spudcan	*Soft clay	0.33D	2.0D	0.55D	Fixed head condition		1.02	13.1	-	-	Effect of global response and large sliding
						Preloading A (K_{ISO})		0.94	13.8	0.49	-0.23	
						Preloading B (K_{LDFE})	ω = 1.0	0.93	13.6	0.55	-0.13	
							ω = 0.5	0.75	13.7	2.67	-0.11	
							ω = 0.3	0.56	13.4	3.98	-0.08	
							ω = 1.0	0.25	12.5	6.23	-0.04	
II	Generic spudcan	#Very Stiff clay	0.66D	1.0D	0.50D	Fixed head condition		7.55	73.0	-	-	Leg damage
						Preloading A (K_{ISO})		6.35	72.0	3.43	-1.37	
III	Novel spudcan	*Soft clay	0.33D	2.0D	0.55D	Preloading B (K_{LDFE})	ω = 1.0	0.64	13.8	0.40	-0.10	Effect of novel spudcan
							ω = 0.1	0.27	12.2	3.72	-0.05	
		#Very Stiff clay	0.66D	1.0D	0.50D	Preloading A (K_{ISO})		4.18	58.2	2.35	1.06	

Note: *Soft clay: $s_{u,ref}$ = 2.4 + 1.35z (kPa) (Menzies & Roper, 2008)
#Very stiff clay: $s_{u,ref}$ = 50.0 (kPa)

Table 3. Displacement and rotation at each location (locations a, b, c and d) at the penetration depth with H_{max} and θ_{max}

		Lateral displacement at δ_{max} (m)					Rotation at θ_{max} (degree)				
		$\Delta\delta_a$	$\Delta\delta_b$	$\Delta\delta_c$	$\Delta\delta_d$	δ_{max}	$\Delta\theta_a$	$\Delta\theta_b$	$\Delta\theta_c$	$\Delta\theta_d$	θ_{max}
Preloading A (K_{ISO})	Measured value	0.00	0.01	0.00	0.48	0.49	0.00	-0.03	-0.03	-0.17	-0.23
	Ratio*	0%	2%	0%	98%	100%	0%	13%	13%	74%	100%
Preloading B (K_{LDFE})	Measured value	0.05	0.25	0.00	0.25	0.55	0.12	-0.08	-0.03	-0.13	-0.12
	Ratio	10%	45%	0%	45%	100%	-100%	67%	25%	108%	100%
Preloading B ($0.5K_{LDFE}$)	Measured value	2.25	0.20	0.00	0.22	2.67	0.09	-0.06	-0.03	-0.11	-0.11
	Ratio	84%	8%	0%	8%	100%	-82%	55%	27%	100%	100%
Preloading B ($0.3K_{LDFE}$)	Measured value	3.65	0.16	0.00	0.17	3.98	0.07	-0.05	-0.02	-0.08	-0.08
	Ratio	92%	4%	0%	4%	100%	-88%	63%	25%	100%	100%
Preloading B ($0.1K_{LDFE}$)	Measured value	6.09	0.07	0.00	0.07	6.23	0.03	-0.02	-0.01	-0.04	-0.04
	Ratio	98%	1%	0%	1%	100%	-75%	50%	25%	100%	100%

Note: *Ratio: $\Delta\delta_{Location} / \delta_{max}$ & $\Delta\theta_{Location} / \theta_{max}$

Table 4. Dimensions and properties for chord and bracing

Dimensions and properties		
Chord	Outer diameter, D_{chord} (cm)	60
	Thickness, t_{chord} (cm)	6
Rack	Length, L_{rack} (cm)	64
	Thickness, t_{rack} (cm)	21
Rack & chord	Area, $A_{r\&c}$ (cm^2)	2362
	Moment of inertia, $I_{r\&c}$ (cm^4)	487817
	Radius of gyration, $r_{r\&c}$ (cm)	14
Brace	Outer diameter, D_{brace} (cm)	20
	Thickness, t_{brace} (cm)	2
Length of bay, L_{bay} (cm)		750
Young's modulus, E_{steel} (MPa)		2.05E+05
Yield stress, σ_{yield} (MPa)		414~700

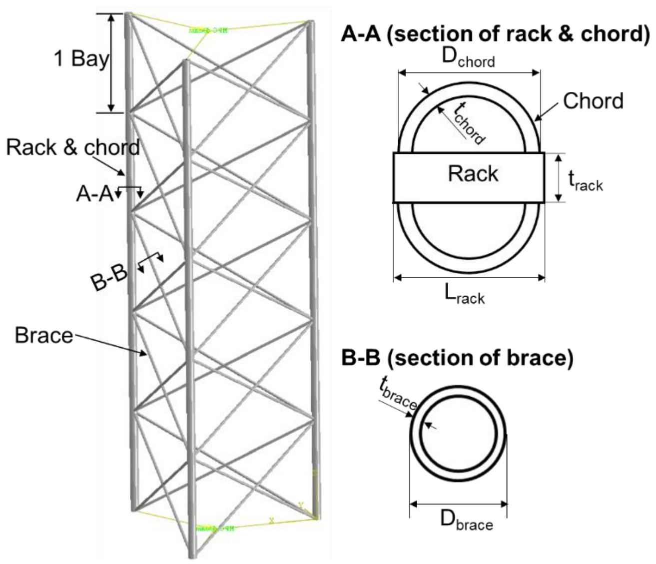

List of Figures

Fig. 15. Detailed structural analysis results on leg just below hull (generic spudcan) in very stiff clay and a deep cylindrical footprint (unit: MPa)

Fig. 16. Resistance forces and spudcan deflections induced by spudcan-footprint interaction (generic, novel and large novel spudcan) in soft clay and a shallow conical footprint for the large deflection case of preloading B (K_{LDFE} vs $0.1K_{LDFE}$): a) Horizontal resistance force; (b) Vertical resistance force; (c) Moment resistance; (d) Lateral displacement; (e) Rotation

Fig. 17. Failure mechanism of the novel spudcan for the large deflection case: (a) d/D = 0.1; (b) d/D = 0.2; (c) d/D = 0.3; (d) d/D = 0.38

Fig. 18. Resistance forces and spudcan deflections induced by spudcan-footprint interaction (generic vs novel spudcan) with a fixed head condition and preloading A (K_{ISO}) in very stiff clay and a deep cylindrical footprint: (a) Horizontal resistance force; (b) Vertical resistance force; (c) Moment resistance; (d) Lateral displacement; (e) Rotation

Fig. 19. Failure mechanism of the novel spudcan for the leg failure case of preloading A (K_{ISO}): (a) d/D = 0.2; (b) d/D = 0.4; (c) d/D = 0.6; (d) d/D = 0.7

Fig. 20. Beam stress and detailed structural analysis of a leg just below the hull for the leg failure case (novel spudcan) (unit: MPa): (a) Structural beam stress of a leg just below the jack-up rig hull with the normalised penetration depth; (b) Detailed structural analysis results of a leg just below the hull